

Breathing Mode in a Pattern-Forming System with Two Competing Lengths

P. E. Cladis,⁽¹⁾ J. T. Gleeson,^{(1),(2),(a)} P. L. Finn,⁽¹⁾ and H. R. Brand⁽³⁾

⁽¹⁾*AT&T Bell Laboratories, Murray Hill, New Jersey 07974*

⁽²⁾*Physics Department, Kent State University, Kent, Ohio 44242*

⁽³⁾*Fachbereich Physik, Universität Essen, D-43 Essen 1, Federal Republic of Germany*

(Received 22 April 1991)

We study interfacial pattern formation during directional growth from the isotropic phase of a cholesteric liquid crystal that, at equilibrium, has a length $2\pi/q_0$. We find an oscillatory first instability to the cellular pattern and a second bifurcation to an oscillatory mode (breathing mode) when the pattern's wave number, q , is $0.5q_0 < q < q_0$. The breathing mode frequency is linear in q . This is the first observation in pattern-forming systems of an oscillatory mode due to competition between two incommensurate but comparable lengths.

PACS numbers: 47.20.Hw, 05.70.Ln, 61.30.-v

The physical characterization of pattern-forming systems has recently received much attention [1]. Directional solidification, the investigation of patterns exhibited by solid-liquid interfaces propagating at speed v in a temperature gradient G/v , is a classic example of such a system that has become one of the preferred systems studied by physicists during the last few years [2]. However, as pattern formation at most solid-liquid interfaces in directional solidification shows behavior similar to strongly first-order phase transitions, it cannot be studied near onset, the region of phase space most amenable to theory. To overcome this difficulty, Libchaber's group [3,4] pioneered directional growth of nematic liquid crystals from the isotropic liquid. As this transition is weakly first order in equilibrium, its interface moving in a temperature gradient has correspondingly small-amplitude patterns with a well-defined wavelength, even far above onset, suggesting the influence of long-range cooperative effects [5]. However, as the pattern amplitude is not small compared to a dynamic impurity diffusion length, interesting nonlinear effects are also observed [4].

Here we consider the influence of an intrinsic length scale on interfacial patterns during directional growth. The materials are cholesteric liquid crystals that, as a consequence of their handedness, at equilibrium have a macroscopic intrinsic length, the helical pitch, $2\pi/q_0$. We describe impressive competing effects that arise when this intrinsic length, $2\pi/q_0$, is comparable to a nonequilibrium length, $2\pi/q$, defined by the pattern's wavelength. In contrast to the nematic case [3] for which $q_0=0$, the onset of the first instability at the cholesteric-isotropic interface is time dependent. There is a second bifurcation to a nonlinear oscillatory pattern that we call a breathing mode. The simple picture to emerge is that the equilibrium cholesteric structure favors a uniform q_0 across the interface while the nonequilibrium driving force creates a spatially periodic elastic stress of wave number q . When q is comparable but incommensurate with q_0 , the elastic response of the ordered state is out of phase with the driving force resulting in an oscillatory mode.

Nematic liquid crystals break continuous rotational symmetry of the isotropic liquid. They are liquid phases with long-range orientational order [6] along a unit vector \mathbf{n} that does not distinguish between head and tail. We study a mixture of the nematic liquid crystal 8CB (cyano-octyl biphenyl) and the chiral impurity C15 [cyano (methyl) butoxybiphenyl] at concentration $c_\infty=9\%$ by weight. The equilibrium structure of this cholesteric liquid crystal [6] is a right-handed helix in which \mathbf{n} spontaneously rotates uniformly about a twist axis, \mathbf{q}_0 , where $\mathbf{q}_0 \perp \mathbf{n}$. The pitch, $p_0=2\pi/q_0$, is the distance for a 2π rotation of \mathbf{n} . Cholesteric liquid crystals break continuous rotational and continuous translational symmetry of the isotropic liquid.

Directional growth patterns with wave number q are driven by spatial variations in impurity concentration c that enable the interface to deviate from a constant temperature surface. Indeed, the pure 8CB used here does not exhibit patterns for $G > 1$ K/cm. For this system, the measured dependence of the transition temperature to the isotropic phase on c is $T_{Ch-I}(\text{°C})=40.36-0.22c(\text{wt.}\%)$. However, the cholesteric pitch p_0 depends on concentration c of a chiral impurity following the linear relation [6,7]: $q_0(\mu\text{m}^{-1})=0.02c(\text{wt.}\%)$. For the c_∞ used here, $q_0=2\pi/p_0=2\pi/(38.5\ \mu\text{m})$. These relations, measured under equilibrium conditions, are accurate to 2%. Thus, by tuning q it is possible to observe competition between the nonequilibrium driving force creating spatial variations in c , and therefore $q_0 \propto c$, and long-range orientational forces favoring a constant q_0 .

The material is between two 1-mm-thick microscope slides prepared [8] with $\mathbf{n} \parallel \hat{z}$ on each slide of $\hat{x}-\hat{z}$ dimensions $26\ \text{mm} \times 40\ \text{mm}$. To allow a uniform 2π twist in \mathbf{n} along \hat{y} , sample thicknesses range from 37 to 41 μm . We selected this particular thickness range and glass-liquid crystal boundary condition to provide defect-free contacts for the cholesteric helical structure at the glass surface [7,9] and to minimize 3D effects that give complicated patterns.

In the experiment, the sample is placed in a fixed con-

stant temperature gradient, $G=7.5 \pm 0.01$ K/cm and $G \parallel \hat{z}$, chosen so that the cholesteric-isotropic interface, viewed along \hat{y} , is visible through an optical microscope. The interface is forced to propagate into the isotropic liquid at a constant speed $v \parallel \mathbf{G}$ by displacing the sample at $-\mathbf{v}$ to colder temperatures. For $v \leq v_c$, the interface profile is parallel to an isotherm (i.e., $\parallel \hat{x}$). Above a critical speed, $v_c = 19 \pm 0.5 \mu\text{m/s}$, there is a bifurcation to a cellular pattern with a well-determined wavelength, $2\pi/q$, the distance between grooves. q depends [10] on both v and G . As q is well defined even when $v \approx 3v_c$, it was determined from the pattern's power spectrum at each speed v .

We scale q by the equilibrium length q_0 because the length for impurity diffusion, l_D , is small in liquid crystals. Taking the impurity diffusion constant in the isotropic liquid as [11] $D_I \sim 4 \times 10^{-7} \text{ cm}^2/\text{s}$, $l_D \equiv D_I/v < 2.1 \mu\text{m} \ll 2\pi/q \sim 130 \mu\text{m}$ when $v \approx v_c$ while $q/q_0 \sim O(1)$. Thus, the equilibrium q_0 is a physically relevant scale for q . Figure 1 shows that q/q_0 is linear in $\epsilon \equiv (v - v_c)/v_c$ for $\epsilon \geq 0.05$.

A striking feature of cholesteric-isotropic patterns is their dynamics on time scales $\gg 1$ s, i.e., longer than the dynamic diffusion time, $D_I/v^2 \leq 0.2$ s. However, orientational diffusion relaxes the gradients in q_0 created by the pattern at the interface. The diffusion constant for this process is $D_0 \equiv K_2/\gamma_1 = 8 \times 10^{-7} \text{ cm}^2/\text{s} \approx 2D_I$. K_2 is a twist elastic constant and γ_1 the rotational viscosity [12]. As $q_0 \neq 0$, both an intrinsic speed, $v_{el} = D_0/\rho_0 \sim 2.1 \mu\text{m/s}$, and frequency, $\omega_{el}/2\pi = D_0 q_0^2 \sim 2 \text{ s}^{-1}$, can be defined.

Space-time plots of groove positions at the first bifurcation for the cholesteric-isotropic interface show the cellular pattern propagating parallel to the interface at speed v_x . Both directions of propagation are observed. *In con-*

trast to the $q_0=0$ case [3], the first instability for the $q_0 \neq 0$ interface is a Hopf bifurcation. Figure 1 shows $v_x/v_{el} \sim O(1)$ is linear in ϵ , but the scaling factor for v_x is sensitive to defect shedding by the interface, as shown by the observation of two linear regimes for v_x vs ϵ in Fig. 1.

For the six data points in the first regime, $0 < \epsilon < 2$, $v_x/v_{el} = 0.32\epsilon + 0.3$ and the orientation of the twist axis \mathbf{q}_0 , determined by the boundary condition, is along \hat{y} only. For the four data points in the second regime, $2.1 < \epsilon < 3.5$, $v_x/v_{el} = 0.60\epsilon + 0.03$, the twist axis \mathbf{q}_0 has two spatial degrees of freedom as evidenced by the formation of λ defects [6,7,13] [Fig. 2(a)] and the helical pattern they form in an $\hat{x}-t$ space-time plot [Fig. 2(b)]. The additional degree of freedom for \mathbf{q}_0 in the second regime correlates with a doubling of the slope in Fig. 1 for v_x/v_{el} vs ϵ when $\epsilon > 2$ compared to $\epsilon < 2$. The two lines cross at $\epsilon \sim 1$ and $q = 0.5q_0$ where the breathing mode starts at a new, second critical speed $v_c^B \approx 2v_c \sim 38.5 \mu\text{m/s}$.

Figure 2(a) is one video frame of the breathing mode

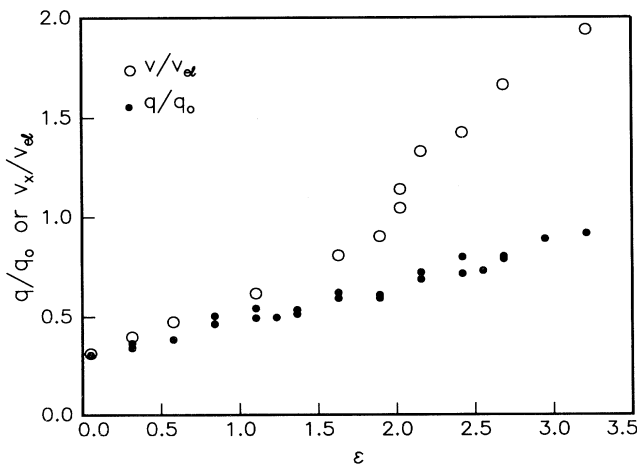


FIG. 1. The wave number q of the cellular pattern scaled by the equilibrium wave number q_0 and the pattern speed v_x parallel to the interface scaled by a speed characteristic of director diffusion and q_0 , $v_{el} = K_2 q_0 / 2\pi\gamma_1$, as a function of the control parameter ϵ .

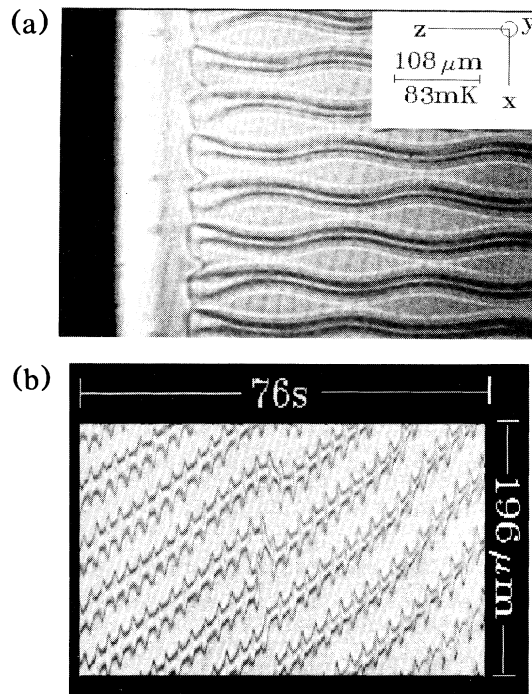


FIG. 2. (a) One video frame showing the breathing-mode pattern decorated behind the interface by disclination lines when $\epsilon_B = 0.56$ viewed with polarizers crossed at 45° to the sides of the frame. The λ defect is seen as the wavy bright line surrounded by two wavy dark lines. The black region at the extreme left is the isotropic phase. The bright band next to it is the cholesteric-isotropic meniscus. Inset: The temperature and length scale as well as the frame of reference used in this paper. (b) Space-time helices of the breathing mode decorated by oscillating λ defects observed when $\epsilon_B = 0.82$: $v = 70.0 \mu\text{m/s}$ and $v_x \approx 3.45 \mu\text{m/s}$.

decorated by an array of λ -defect lines shed by the interface [13] in the regime $2 < \epsilon < 3.5$. In Fig. 2(a), $v = 60 \mu\text{m/s}$ or $\epsilon_B \equiv (v - v_c^B)/v_c^B = 0.56$. Oscillations of neighboring lines are in antiphase whereas next-nearest neighbors are in phase. In the uniform region between the lines, $\mathbf{q}_0 \parallel \hat{\mathbf{y}}$. While the defect oscillatory motion is nearly 1D at $\epsilon_B = 0.56$ [Fig. 2(a)] where the oscillation amplitude is maximum, it is observably 2D at $\epsilon_B = 0.82$ as shown by the space-time helices (and a dislocation) in Fig. 2(b). The space-time plot is obtained by capturing a single video line parallel to $\hat{\mathbf{x}}$ just behind the interface every 0.25 s then replotted the lines in sequence. Although an oscillatory mode was predicted for incommensurate pattern forming systems far above onset [14], this is the first time such a mode has been observed resulting from competition between equilibrium and nonequilibrium forces [15].

In the breathing mode, the oscillation amplitude measured parallel to x grows from zero at $\epsilon \sim 1$ when $v \sim 40 \mu\text{m/s}$, peaks (largest measured amplitude was $\sim 27 \mu\text{m} \sim 1.5\pi/q_0$) at $\epsilon \sim 2$, then decreases to zero when $\epsilon \sim 3.2$ and cells are no longer visible defining an upper critical speed [10] $v_c^u \sim 80 \mu\text{m/s}$. Because of a coupling [6,16,17] between \mathbf{q}_0 and \mathbf{v} , when $\epsilon > 3.5$, the helix again rotates [18] so that $\mathbf{q}_0 \parallel \mathbf{v}$. At even larger v , a coherent helix structure no longer forms [18]: $q_0 = 0$.

A feature of the breathing mode is that alternate grooves grow while nearest neighbors shrink giving an alternating chain of large and small grooves doubling the pattern wavelength (i.e., halving the wave number plotted in Fig. 1). A video line parallel to $\hat{\mathbf{x}}$, crossing the array of longer grooves but not the array of shorter ones, is cap-

tured every ~ 0.3 s then replotted in sequence. The binarized example in the inset of Fig. 3 taken at $\epsilon_B = 0.1$ shows the pattern in a standing-wave mode. The dispersion relation for the driven breathing model is obtained by Fourier transforming the $x-t$ plots to obtain a structure factor, $S(q, \omega)$. In Fig. 3, $q/2$ is scaled by q_0 and the oscillation frequency, ω , by a characteristic frequency for director diffusion, $\omega_{el} = 2\pi D_0 q_0^2 = q_0(84 \mu\text{m/s})$. The best line to the data is $\omega/\omega_{el} = -0.23 + 1.13q/2q_0$ with a group velocity $v_g = 95 \mu\text{m/s} \gg v_{el}$: The breathing mode is nondispersive and nonlinear. Occasionally a group of breathing cells travels parallel to $\hat{\mathbf{x}}$ at speeds large compared to v_{el} in an excitation similar to the "solitons" of Simon, Bechhoefer, and Libchaber [4]. Space-time plots at $40 \mu\text{m/s}$ showed soliton speeds ranging from 12 to $16 \mu\text{m/s} \sim K_2 q_0 / \gamma_1 < v_g$. The large value for v_g deduced from Fig. 3 is a measure of the decisive role played in this pattern by the nonequilibrium driving force.

We digitized a series of frames of the breathing mode to extract the variation in elastic energy in one breathing cycle. Three such frames captured at $t/T = -0.4, 0,$ and 0.4 are shown in Fig. 4 with the digitized profiles, $z_I(x)$, superimposed. Here $v = 50 \mu\text{m/s}$. The breathing-mode period is $T = 4.7 \pm 0.02$ s and its wavelength is $124 \mu\text{m}$.

Because conservation of impurities requires impurity deficit from c_∞ in the tip region be balanced by impurity excess in a groove, we integrate $z_I(x)$ for each frame to find z_∞ corresponding to c_∞ . The cholesteric elastic energy is then proportional to $(z_I - z_\infty)^2$, shown as the white curves plotted on the black strip below each frame. Here we see that the elastic energy associated with the larger grooves towers above that of the smaller ones where it is

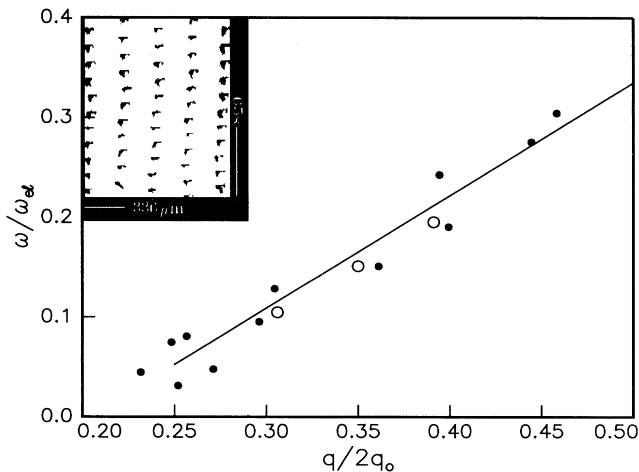


FIG. 3. Dispersion curve for the breathing mode. The frequency ω is scaled with an elastic frequency ω_{el} and $q/2$ by q_0 . The sample thicknesses are $41 \mu\text{m}$ (●) and $37 \mu\text{m}$ (○). To within experimental uncertainty, the breathing-mode group velocity is a constant and $95 \mu\text{m/s} \gg v_{el}$. Time increases upward for the 2D space-time crystal shown in the inset.

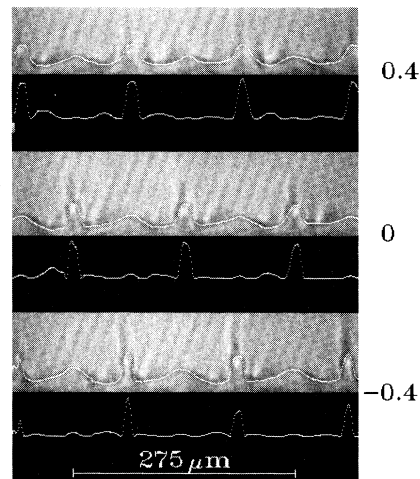


FIG. 4. Video frames of the breathing mode for $t/T = -0.4, 0,$ and 0.4 , where T is the period of the mode measured to be 4.7 ± 0.02 s at $v = 50 \mu\text{m/s}$. The digitized profiles, $z_I(x)$, are overlaid in each frame. The variation in elastic energy density across the interface, deduced from $z_I(x)$, is shown in the black region below each frame.

nearly zero just before the next period. A simple picture to emerge is that the equilibrium elastic energy in the cholesteric phase favors a uniform q_0 across the interface. Because the nonequilibrium driving force creates a spatially periodic elastic stress of wave number q , where $q_0 > q > 0.5q_0$, the slower elastic response of the ordered state is out of phase resulting in an oscillatory mode.

We note that a nonlinear oscillatory mode, presumably also arising from competition between two lengths, has recently been observed over parts of Al-Cu alloys close to the eutectic [19]. However, its length scale is more than 4 orders of magnitude smaller than observed here so it must be investigated by electron microscopy instead of optical microscopy and time-resolved studies are more difficult. As the cholesteric-isotropic system is transparent and its pattern-forming aspects can be easily investigated in space and time, its study may help understand the origin of similar patterns in the experimentally more difficult metallurgical systems.

In conclusion, the existence of an intrinsic length $2\pi/q_0$ in cholesteric liquid crystals can give rise to a frequency of the response of interfacial patterns with wave number q to perturbations from the equilibrium structure. After carefully choosing boundary conditions and sample dimensions, we tuned q and explored the regime $q \sim q_0$. In this regime, the first instability to the cellular pattern is a Hopf bifurcation. A frequency is not associated with the cellular bifurcation when $q_0 = 0$. A second bifurcation to a nonlinear breathing mode is observed when $0.5q_0 < q < q_0$.

We thank Alain Karma for drawing our attention to Ref. [19]. This work was partially supported by NATO CRG 890777. H.R.B. thanks the Deutsche Forschungsgemeinschaft and J.T.G. thanks NSERC (Canada) for support.

^(a)Present address: Department of Physics, Princeton University, Princeton, NJ 08544.

- [1] See, for example, *Nonlinear Evolution of Spatio-Temporal Structures in Dissipative Continuous Systems*, edited by F. H. Busse and L. Kramer (Plenum, New York, 1990).
- [2] J. S. Langer, *Rev. Mod. Phys.* **52**, 1 (1980).
- [3] J. Bechhoefer, A. J. Simon, A. Libchaber, and P. Oswald, *Phys. Rev. A* **40**, 2042 (1989).
- [4] A. J. Simon, J. Bechhoefer, and A. Libchaber, *Phys. Rev. Lett.* **61**, 2574 (1988).
- [5] P. Palfy-Muhoray has suggested that a length relevant for pattern formation in Ref. [3] could be K/σ , where K is a nematic elastic constant and σ the surface energy.
- [6] P. G. de Gennes, *The Physics of Liquid Crystals* (Clarendon, Oxford, 1982), 3rd ed.
- [7] P. E. Cladis and M. Kléman, *Mol. Cryst. Liq. Cryst.* **16**, 1 (1972).
- [8] J. S. Patel, T. M. Leslie, and J. W. Goodby, *Ferroelectrics* **59**, 137 (1984).
- [9] In P. Oswald, J. Bechhoefer, A. Libchaber, and F. Lequeux, *Phys. Rev. A* **36**, 5832 (1987), as well as other previous work on nematics, using the frame of reference introduced here, samples are prepared with $n\parallel\hat{y}$.
- [10] This compares well with measurements by A. J. Simon and A. Libchaber, *Phys. Rev. A* **41**, 7090 (1990), for nominally pure 8CB in a similar temperature gradient.
- [11] M. Hara, H. Takezoe, and A. Fukuda, *Jpn. J. Appl. Phys.* **25**, 1756 (1986). These authors find the average impurity diffusion constant in the cholesteric liquid, $D_{\text{avg}} \sim 2 \times 10^{-7} \text{ cm}^2/\text{s} \sim D_l/2$.
- [12] We take $K_2 = 2 \times 10^{-7} \text{ dyn}$ from the measurement of M. J. Bradshaw, E. P. Raynes, J. D. Bunning, and T. E. Faber, *J. Phys. (Paris)* **46**, 1513 (1985). Although these authors do not measure K_2 in 8CB, we assume that in the vicinity of the isotropic phase, the one-constant approximation ($K_1 = K_2 = K_3$) holds. We take $\gamma_1 = 0.25 \text{ dyn}/(\text{cm}^2/\text{s})$ from H. Knepe, F. Schneider, and N. K. Sharma, *J. Chem. Phys.* **77**, 3203 (1982).
- [13] λ defects, also called "double twist" by S. Meiboom, J. P. Sethna, P. W. Anderson, and W. F. Brinkman, *Phys. Rev. Lett.* **46**, 1216 (1981), because the twist axis has two spatial degrees of freedom, are observed along \hat{y} as periodic variations in the extraordinary index of refraction along \hat{x} . No change in the uniform cholesteric texture grown at $\epsilon < 2$ is observed when $v \rightarrow 0$ showing that the twist axis was indeed defined by boundary conditions, i.e., $q_0\parallel\hat{y}$ only. In contrast, λ defects formed when $\epsilon > 2$ slowly disappeared when $v \rightarrow 0$. When $1 < \epsilon < 2$, defect shedding by the interface is less frequent (generally stimulated by dust particles) and is of the $\chi = \frac{1}{2}$ type [6,7] with $q_0\parallel\hat{y}$.
- [14] H. R. Brand, *Phys. Rev. A* **32**, 3551 (1985).
- [15] The breathing mode is reminiscent of, but distinct from, the subtle optical mode reported in nematics by J. M. Flesselles, A. J. Simon, and A. Libchaber, *Adv. Phys.* **30**, 1 (1991). Although cholesterics and nematics have the same orientational diffusion constant, the intrinsic dynamic scales introduced here cannot be defined for nematics for which $q_0 = 0$.
- [16] H. R. Brand and H. Pleiner, *Phys. Rev. A* **37**, 2736 (1988).
- [17] J. L. Ericksen, *Arch. Rational Mech. Anal.* **113**, 97 (1991).
- [18] H. R. Brand and P. E. Cladis (to be published).
- [19] M. Zimmermann, A. Karma, and M. Carrard, *Phys. Rev. B* **42**, 833 (1990). To underscore the generic aspect of the breathing mode, we note that a pattern similar to the breathing mode [Fig. 2(a)] has been observed in eutectic systems. A distinct advantage of our system over metallurgical systems is that, in our system, the pattern's time evolution can be followed.

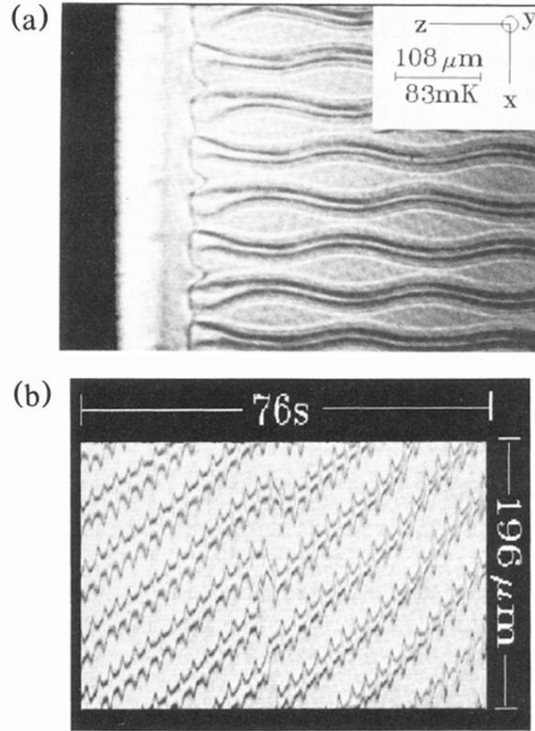


FIG. 2. (a) One video frame showing the breathing-mode pattern decorated behind the interface by disclination lines when $\epsilon_B=0.56$ viewed with polarizers crossed at 45° to the sides of the frame. The λ defect is seen as the wavy bright line surrounded by two wavy dark lines. The black region at the extreme left is the isotropic phase. The bright band next to it is the cholesteric-isotropic meniscus. Inset: The temperature and length scale as well as the frame of reference used in this paper. (b) Space-time helices of the breathing mode decorated by oscillating λ defects observed when $\epsilon_B=0.82$: $v=70.0 \mu\text{m/s}$ and $v_x \approx 3.45 \mu\text{m/s}$.

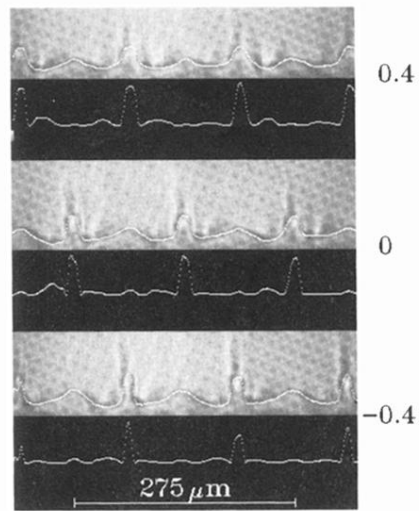


FIG. 4. Video frames of the breathing mode for $t/T = -0.4$, 0, and 0.4, where T is the period of the mode measured to be 4.7 ± 0.02 s at $v = 50 \mu\text{m/s}$. The digitized profiles, $z_l(x)$, are overlaid in each frame. The variation in elastic energy density across the interface, deduced from $z_l(x)$, is shown in the black region below each frame.